Custom Beamsplitter and AR Coatings for Interferometry

K. Nyland[a], C.A. Jurgenson[a], D.F. Buscher[b], C.A. Haniff[b], J.S. Young[b], J. Lewis[c], R. Schnell[c]

[a]New Mexico Institute of Mining and Technology, Magdalena Ridge Observatory, 101 East Road, Socorro, NM 87801;
[b]University of Cambridge, Cavendish Laboratory, Dept. of Physics, JJ Thomson Avenue, Cambridge, CB3 OHE, UK;
[c]Optical Surface Technologies, 2801 Unit E Broadbent Parkway N.E., Albuquerque, NM 87801, USA

ABSTRACT

We report on final fabrication tests for the dielectric coatings for the Magdalena Ridge Observatory Interferometer (MROI) fringe tracking beam combiner. The broadband anti-reflection (1.1 μm to 2.4 μm) and beamsplitter (1.49 μm to 2.31 μm) coatings required have been designed with both optical and mechanical constraints in mind. Not only do these coatings have very low optical losses, but they induce minimal bending of their substrates, thereby giving very low fringe contrast reductions. Performance tests on the deposited coatings at our manufacturers (Optical Surface Technologies, Albuquerque, NM) demonstrate reflection losses of less than 0.5% over the full bandpass of the AR coating, and deviations from the desired 50:50 intensity ratio of the beamsplitter coating of no more than 2%. When combined with the measured wavefront perturbations these results imply that the total fringe visibility losses induced by imperfect coating quality will be no more than 2% for all outputs of the MROI fringe tracking beam combiner.

Keywords: MROI, interferometry, beamsplitter, anti-reflection (AR), coatings, baseline bootstrapping

1. INTRODUCTION

The Magdalena Ridge Observatory Interferometer (MROI) will consist of 10 x 1.4 m telescopes optimized for broadband imaging in the H (1.49-1.78 μm) and K_s (1.99-2.31 μm) bands.[1] It will have three beam combiners upon completion: the beam combiner for fringe tracking (FT)[2] and two others for science. The FT requires high throughput and fringe visibility contrast and is critical for the operation of the science combiners. In order to achieve the required performance for the FT, high quality optical coatings are necessary.

All coatings have been custom-designed for interferometric applications. Unlike optical coatings used in more general applications, the coatings used in the FT can precisely control both amplitude and phase variations across very broad bandpasses (1.1-2.4 μm for the AR coatings and 1.49-2.31 μm for the beamsplitters). The performance of two of the dielectric coatings (the AR and 50% beamsplitter coatings) has been tested and compared to stringent design specifications. The results of these measurements and their impact on the interferometric performance of the FT have been analyzed and are presented throughout this paper.

2. THE FRINGE TRACKER BEAM COMBINER

The FT must be able to achieve high throughput and excellent fringe visibility contrast in broadband light. The architecture of a combiner always imposes some performance limitations. Even in the idealized case of perfect optical components and coatings, a combiner cannot provide 100% throughput and fringe visibilities (see Section 4.1 and Figure 5). Figure 1 illustrates the pairwise nature of the combiner with each output containing signals from two telescopes. In this schematic, light from 10 unit telescopes enters at the symmetric combiner at the upper left and exits at the two combiner outputs at the bottom left and right. These outputs are complimentary and exit the combiner π-radians out of phase with one another. Both outputs are labeled in Figure 1 and refer to light that has been right-reflected, left-transmitted (RR-LT) for Combiner Outputs 1 and left-reflected, right-transmitted (LR-RT) for Combiner Outputs 2. Figure 2 shows a detailed view of the two combiner output

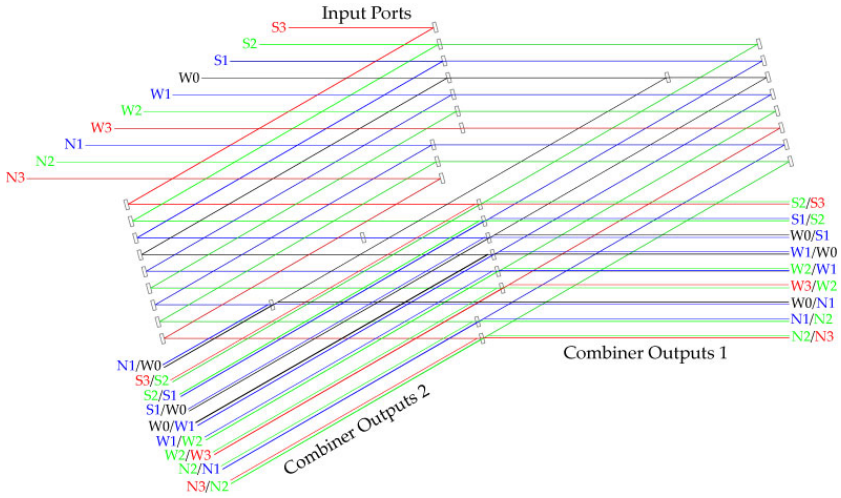

Figure 1. Schematic of the symmetric FT beam combiner layout showing inputs and outputs from all 10 telescopes. Beams enter from the top left and exit at the bottom right and left in pairs π-radians out of phase labeled Combiner Outputs 1 and Combiner Outputs 2.

pairs at the 50% beamsplitter combination point. It is evident from the figure that asymmetries arise because reflections and transmissions occur at different dielectric layers within the beamsplitter.

Since beams in the combiner traverse individual optical components in different directions and in different orders, there exist 8 unique paths (A through H) through the combiner which comprise six non-redundant combination pairs: A-B, C-B, D-E, F-B, C-G and C-H. Figure 3 displays the detailed, and generally asymmetric, paths of each distinct combination pair. The detected fringe visibility at each combiner output of each combination pair depends on the details of the path traversed such as the type of optical components, the number of interactions with a particular component, and the type of coatings encountered. Section 4 describes in detail the effective fringe visibilities for the six pairs due to four visibility loss factors.

3. OPTICAL SYSTEM DESIGN AND PERFORMANCE

3.1 Fabrication

Infrasil 301 was the substrate material chosen for all beamsplitter and compensator plates within the beam combiner based on its unique, high transmissivity in the K-band. The high quality combiner substrates were produced by IC Optical Systems (UK) and were made to adhere to strict manufacturing tolerances (Table 1). For the purposes of this paper, the optical path difference (OPD) in Table 1 is the parameter most relevant to the calculation of fringe visibility losses. It was required that the un-coated substrates introduce an OPD not greater than $\lambda/20$ upon transmission or reflection. Table 1 shows that this manufacturing requirement was indeed met.

3.2 Custom coatings

All substrate coatings were applied by Optical Surface Technologies (Albuquerque, NM) and consist of alternating layers of Nb_2O_5 and SiO_2. There are three distinct coatings: (1) Anti-reflection (AR) coating, (2) 33.33% reflectance beamsplitter coating and (3) 50% reflectance beamsplitter coating. Two of these three coatings have been applied to the substrates (the AR and 50% beamsplitter coatings) and one is still being processed (the 33% beamsplitter coating). In order to help minimize phase errors as well as reduce substrate bending during coating application, as few layers as possible of each custom coating were used. The AR coating is comprised of 5 layers with a total thickness of 1600 nm, the 33.33% beamsplitter coating is comprised of 8 layers with a total

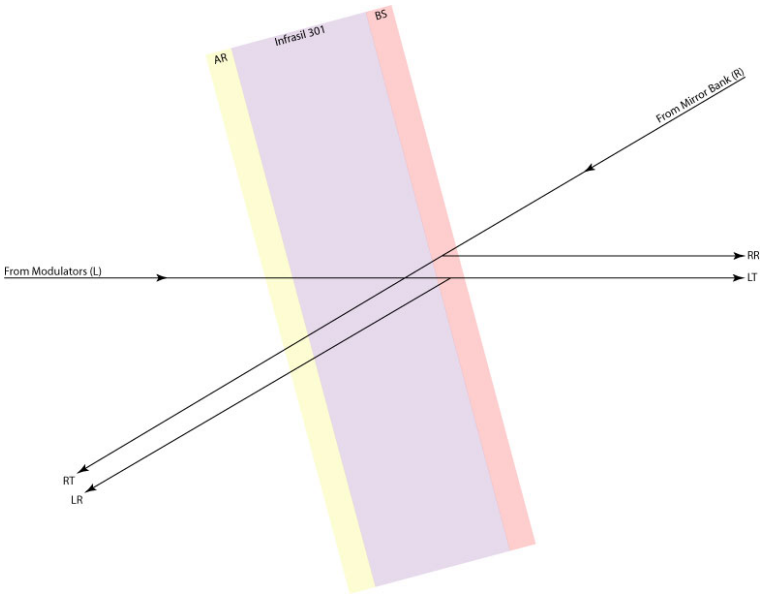

Figure 2. Optical paths at the 50% beamsplitter combination point. There are two complimentary outputs after beam combination: RR-LT and LR-RT. These outputs are π-radians out of phase with one another due to differences in the locations where reflections and transmissions occur within the dielectric coating.

Table 1. The required and measured combiner optic manufacturing tolerances. The parameter relevant to the calculation of fringe visibility losses in this paper is the OPD.

Parameter	Diameter (mm)	Thickness (mm)	Clear Aperture (%)	OPD (at 633 nm)	Parallelism (")	Thickness Matching (μm)	Surface Quality
Required	30±0.1	10±0.1	>85%	$\lambda/20$	<30"	±2.5	40-20
Measured	30.05±0.02	10.09±0.001	>95%	$\lambda/20$	<0.5"	±1	confirmed

thickness of 1800 nm and the 50% beamsplitter coating is comprised of 10 layers with a total thickness of 1800 nm.

The AR coatings were applied to both sides of the compensator plates and one side of each beamsplitter plate. Only one plate received the 33.33% reflective coating; the first beamsplitter encountered by the central telescope. The AR coating was optimized for operation in the J, H and K bands (1.1 μm to 2.4 μm) and can be used by the FT as well as the two other beam combiners. The beamsplitter coatings were optimized for operation in the H and K_s bands (1.49 μm to 2.31 μm) and are only used by the FT.

3.3 Performance

The performance of the coatings in terms of the mean reflectance as a function of wavelength was measured and the results are shown in Figure 4. The data points for the AR and 50% beamsplitter coatings were measured while the graph for the 33.33% beamsplitter coating represents theoretical values only. Note that although the AR coating was designed to operate across the entire J, H and K bands, performance measurements were only obtained for the bandpass spanning 1.5-2.4 μm. From the plots in Figure 4 it is evident that all coatings are performing near specification levels, with mean reflectance deviations within 2% for the 50% beamsplitter coating and 0.5% for the AR coating.

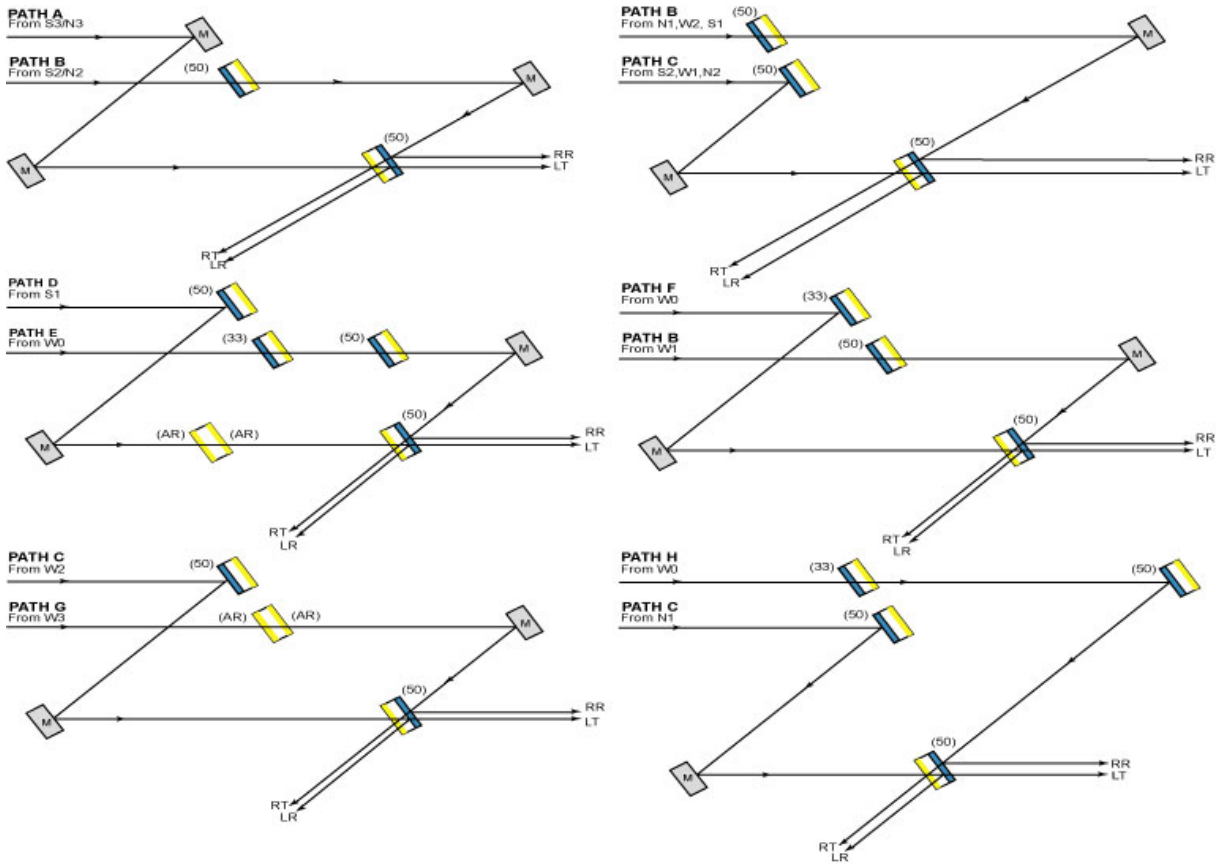

Figure 3. The six non-redundant combination pairs through the FT beam combiner. From top to bottom, pair A-B, C-B, F-B, D-E, C-G and C-H. The optical components labeled on the schematic are gold mirrors (M), 33.33% and 50% beamsplitters (labeled 33 and 50, respectively) and compensator plates (AR AR). The AR coating has been applied to one side of each beamsplitter and both sides of the compensator plates.

4. VISIBILITY LOSS FACTORS

In any real beam combiner, there are many factors which can reduce fringe visibility contrast. These visibility losses are undesirable since they can reduce the combiner signal-to-noise ratio. Of the many visibility loss factors, we have considered four in this paper. These loss factors are (1) intensity mismatch ($V_{mismatch}$), (2) phase offsets due to polarization (V_{pol}), (3) wavefront errors at the substrate and coating surfaces (V_{wfe}) and (4) phase offsets due to group delay (V_{gd}). In the following subsections we calculate these visibility loss factors[3] explicitly for all paths and outputs of the fringe tracker beam combiner. It should be noted again that coating parameters used in the visibility loss calculations were measured for interactions with the AR and 50% beamsplitter coatings but derived theoretically for the 33.33% beamsplitter coating.

4.1 Intensity Mismatch

In an ideal, pairwise beam combiner, the reflected and transmitted components of interfering beams would have equal intensities and there would be no reduction in fringe visibility contrast due to intensity mismatch. In a real beam combiner, however, visibility losses due to intensity mismatch are the result of two effects: (1) the system architecture and (2) coating imperfections. It is the architecture of the beam combiner itself which leads to the greatest reductions in fringe visibility contrast.

The array geometry and the baseline bootstrapping technique[4] used to phase up the arms of the array determine the combiner architecture. Figure 5 shows a schematic of the telescope layout. Individual telescopes

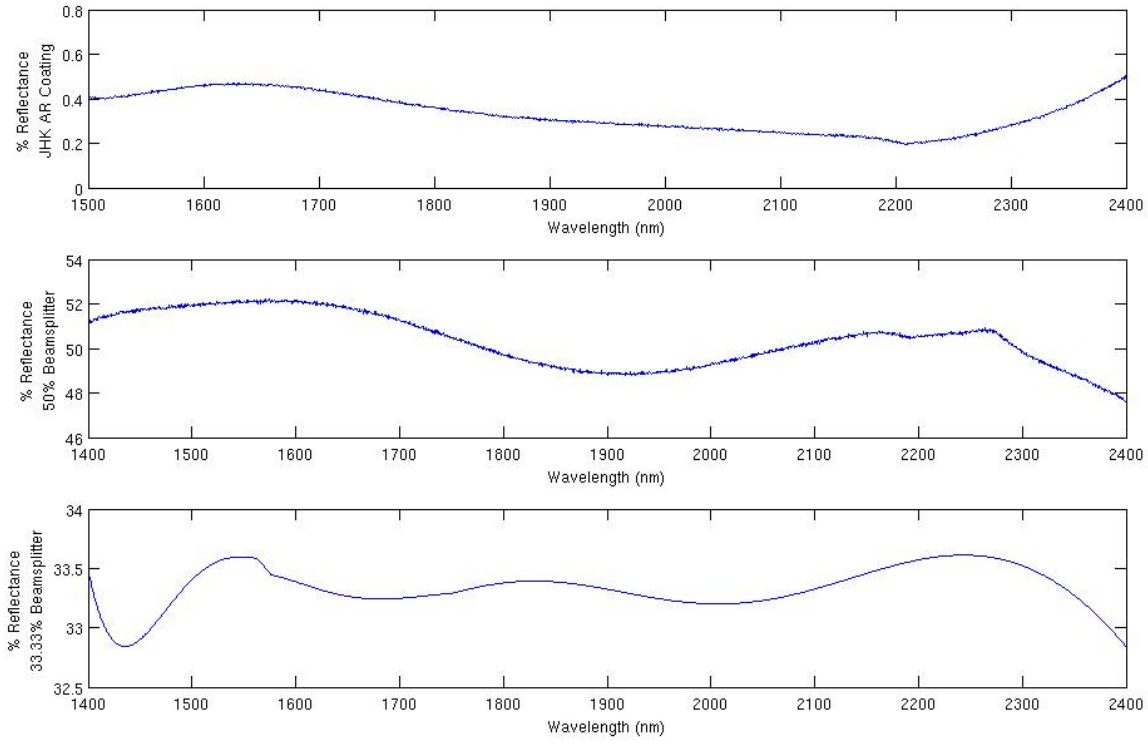

Figure 4. The mean reflectance of the JHK AR and the 50% and 33.33% beamsplitter coatings as a function of wavelength. Note that values for the 33.33% beamsplitter coating are theoretical whereas values for the AR and 50% beamsplitter coatings were measured.

are numbered 0 (central), 1 (inner), 2 (middle) and 3 (outer) within a given arm N (north), S (south) and W (west). The arrows represent the nearest neighbor combinations that are made to bootstrap the array inwards towards the central telescope. The bootstrapping technique dictates the number of combination partners a particular telescope has. Each of the outer telescopes (labeled 3 in Figure 5) have only one combination partner, the inner telescopes (labeled 1 and 2) have two combination partners and the central telescope (labeled 0) has three combination partners. Light is split equally amongst combination partners. This results in differing throughput intensities within the beam combiner and ultimately intensity ratios between paths that are not all equal to unity. For example, when light from telescope S3 combines with light from S2 there is an intensity ratio of 2:1. This results in the largest reduction of fringe visibilities due to the architecture itself (∼94%, Equation 1).

The second cause of visibility losses due to intensity mismatch is imperfections in the dielectric coatings. These imperfections reside in the inability of the coatings to split incoming light exactly as specified (Figure 4). The result is an unequal ratio between the intensity of the reflected and transmitted rays at a particular combiner output. Formally, this intensity ratio is defined as ρ=I_{refl}/I_{trans} where I_{refl} and I_{trans} are the reflected and transmitted throughput intensities, respectively. The intensity ratio is used to calculate the visibility losses due to intensity mismatch in Equation 1 below. These losses are due to the combined effect of the architectural and coating properties and are plotted for all outputs and pairs in Figure 6. In this figure, variations in $V_{mismatch}$ for a particular combiner output are due to architectural path differences in the beam combiner. Variations in $V_{mismatch}$ between combiner outputs for a given combination pair, however, are due to differences in the coating properties of different optical components. Overall, intensity mismatch effects range from 0% to 8% and are responsible for the most significant contribution to visibility losses of all of the loss factors considered here.

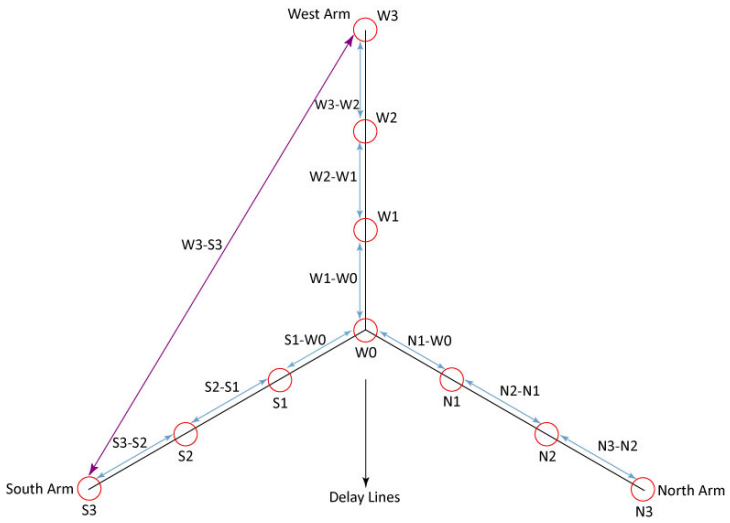

Figure 5. A schematic illustrating the telescope layout and the baseline bootstrapping technique at the MROI. The characteristics of this array geometry, as well as the bootstrapping technique, determine the combiner architecture. The beam combiner makes nearest neighbor combinations which actually lead to inherent reductions in fringe visibility contrast due to intensity mismatch effects.

$$V_{mismatch} = \frac{2}{\rho^{1/2} + \rho^{-1/2}} \tag{1}$$

4.2 Wavefront Error

The second factor contributing to visibility losses is wavefront error. Wavefront errors are the result of substrate or coating imperfections in the combiner optics. Prior to applying the dielectric coatings to the substrates, the effect of the coating application process on the substrate material was tested. This test utilized a 1 mm thick witness sample of the substrate material to measure the surface RMS before and after coating application. Figure 7 shows phase maps of this thin witness sample (a) before and (b) after a coating was applied. The surface RMS before coating application was 0.017 wavelengths and after the coating was applied a surface RMS of 0.024 wavelengths was measured. The total change in surface RMS was 0.041 wavelengths, or $\lambda/24.4$. The results of this test demonstrated that the surface RMS for even a thin, coated sample of the substrate met the design requirements (deviations of no more than $\lambda/20$ wavelengths). This test also showed that bending due to coating application on even a thin substrate sample is small. Since the actual substrates used in the fringe tracker are 10 mm thick, bending effects are even smaller in practice.

Equations 2-5 were used to calculate the wavefront errors for the interactions due to the individual optical components. In these equations δ_m, δ_{bsr}, δ_{bst} and δ_c refer to interactions with a mirror, a beamsplitter reflection, a beamsplitter transmission and a compensator plate, respectively. The RMS terms refer to the measured deviations from flatness averaged across each corresponding optical component (RMS_m=0.008, $\text{RMS}_{bsr}=\frac{0.023}{\sqrt{2}}$, RMS_{bst}=0.023 and RMS_c=0.014). The cosine projection factor is necessary since the optical components are tilted 15^o with respect to normal beam incidence. The final two parameters in Equations 2-5 are the reference wavelength of 633 nm (λ_0) and the index of refraction, n, of the material.

$$\delta_m = 2 * RMS_m * \lambda_0 * \cos(15^o) \tag{2}$$

$$\delta_{bsr} = 2 * RMS_{bsr} * \lambda_0 * \cos(15^o) \tag{3}$$

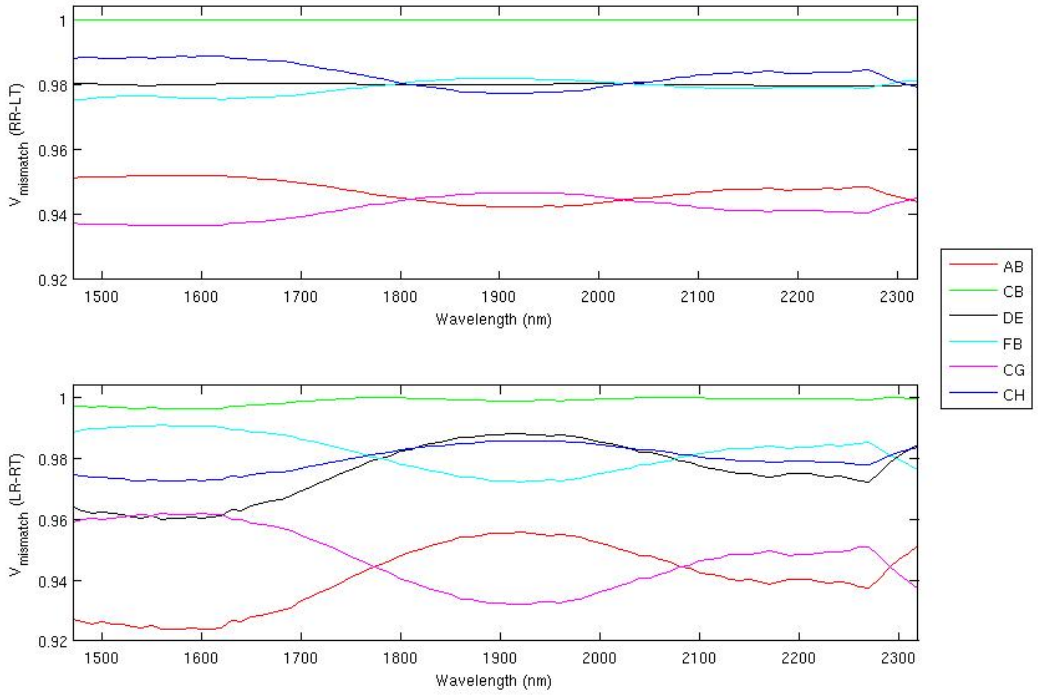

Figure 6. The visibility loss factors as a function of wavelength due to intensity mismatch calculated using Equation 1 for the two combiner outputs (top) RR-LT and (bottom) LR-RT.

$$\delta_{bst} = RMS_{bst} * \lambda_0 * \sqrt{(n^2 - \sin(15^o)^2) - \cos(15^o)} \tag{4}$$

$$\delta_c = RMS_c * \lambda_0 * \sqrt{(n^2 - \sin(15^o)^2) - \cos(15^o)} \tag{5}$$

Equation 6 defines the ray wavefront error (δ_r) for each of the four rays (RR, LT, LR, RT). Here, N_m, N_{bsr}, N_{bst} and N_c refer to the number of interactions with a mirror, beamsplitter reflection, beamsplitter transmission and a compensator plate, respectively.

$$\delta_r = \sqrt{N_m * \delta_m^2 + N_{bsr} * \delta_{bsr}^2 + N_{bst} * \delta_{bst}^2 + N_c * \delta_c^2} \tag{6}$$

The total wavefront error, δ, for each of the two combination outputs (RR-LT and LR-RT) was found by adding the wavefront error of each constituent ray in quadrature. This process is defined in Equation 7. The wavefront errors at the RR-LT and LR-RT outputs were found to be identical for all combination paths due to symmetry. Figure 8 shows how the wavefront error itself varies for the reflected and transmitted portions of each combiner path. Total wavefront errors are shown to be at best 19.17 nm and at worst 31.45 nm.

$$\delta = \sqrt{\delta_r(RR)^2 + \delta_r(LT)^2} \tag{7}$$

We used equation 8 below to calculate the visibility loss factors due to wavefront error. These loss factors were found to be small (<2%, Figure 9) for all combiner outputs and pairs.

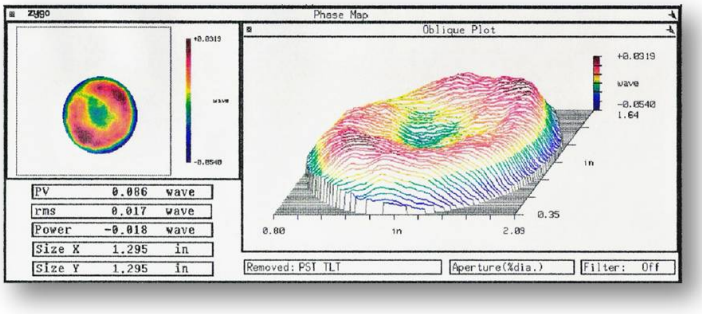

(a) Before coating application.

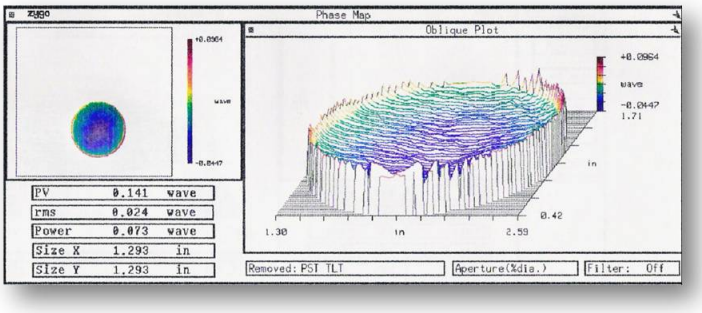

(b) After coating application.

Figure 7. Phase maps of a 1 mm thick witness sample (a) before and (b) after coating application. The total change in the surface RMS between (a) and (b) is $\lambda/24.4$ wavelengths.

$$V_{wfe} = e^{-\frac{(2\pi\delta/\lambda)^2}{2}} \tag{8}$$

4.3 Polarization

The third visibility loss effect considered in this paper is polarization. For a pairwise beam combiner, offsets between the interference patterns of the s and p polarization states at the detector lead to a reduction in fringe visibility contrast. We used Equation 9 to calculate the polarization visibility loss factors for each combiner output of each combination pair. The relative phase, ϕ_{sp}, in Equation 9 is defined as ϕ_{sp}= ϕ_s-ϕ_p and represents the net offset between fringes in the s and p polarization states at a given detector output. ϕ_s and ϕ_p represent the phase of the fringes in the s and p polarizations, respectively. Figure 10 shows a plot of the visibility losses due to polarization effects as a function of wavelength. These visibility losses are extremely small, <0.10% (Figure 10), for all combiner outputs and pairs. In fact, polarization effects account for the smallest contribution to fringe visibility contrast reductions of all of the factors considered in this paper.

$$V_{pol} = |\cos(\frac{\phi_{sp}}{2})| \tag{9}$$

4.4 Group Delay

The final visibility loss factor considered is group delay. Similarly to polarization visibility losses, group delay losses result from phase offsets between interfering beams at the detector. Group delay phase offsets in the fringe tracker are a result of polychromatic light traveling through different amounts of dispersive media with differing

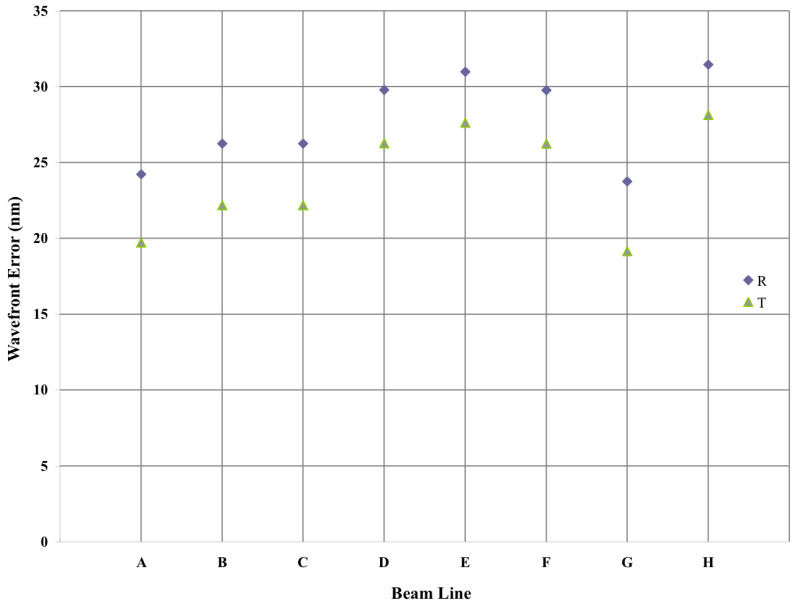

Figure 8. The total wavefront error for each of the eight combiner paths shown for reflected (R) and transmitted (T) light. All values meet the minimum design tolerance of $\lambda/20$ nm.

indices of refraction. Since the index of refraction of a given dispersive material is a function of wavelength, different wavelengths will propagate at different speeds through a given beam combiner path. This results in a delay in polychromatic light arrival times for different wavelengths, which manifests itself as a phase shift. If the rate of change of this phase shift is constant with respect to wavelength then the group delay is constant.

We have calculated the group delay visibility loss factors using Equation 10 below. In this equation a spectral resolution of R=30 was assumed and the corresponding coherence lengths (for the central spectral channels in the H and K_s bands) were $\Lambda_{coh}(H)$=49.5 μm and $\Lambda_{coh}(K_s)$=64.5 μm. The phase offset between fringes due to group delay for a given polarization is denoted as δ_{gd}. These δ_{gd} values were computed at the central spectral channel for the H and K_s bands (λ_c(H)=1.635 μm and $\lambda_c(K_s)$=2.15 μm, respectively) as well as at the midpoint of the upper end channel for these bands (λ'(H)=1.751 μm and $\lambda'(K_s)$=2.278 μm). Since it is the change in group delay across a bandpass which degrades fringe visibility, we calculated the differences (denoted Δ_H and Δ_{Ks}) between the phase offsets at the central and end spectral channels of a each band. This phase offset difference was used in the group delay visibility loss calculation for each polarization of each output for a given combination pair. The results are shown shown in Table 2 and reveal that visibility losses due to group delay are small (<0.8%).

$$V_{gd} = \frac{\sin(\pi \frac{\Delta}{\Lambda_{coh}})}{\pi \frac{\Delta}{\Lambda_{coh}}} \,. \tag{10}$$

5. EXPERIMENTAL VS. IDEAL VISIBILITY

In this paper we have examined four important visibility loss factors and calculated their effects for the MROI fringe tracking beam combiner. It is the combined effect of all of these factors which determines the performance

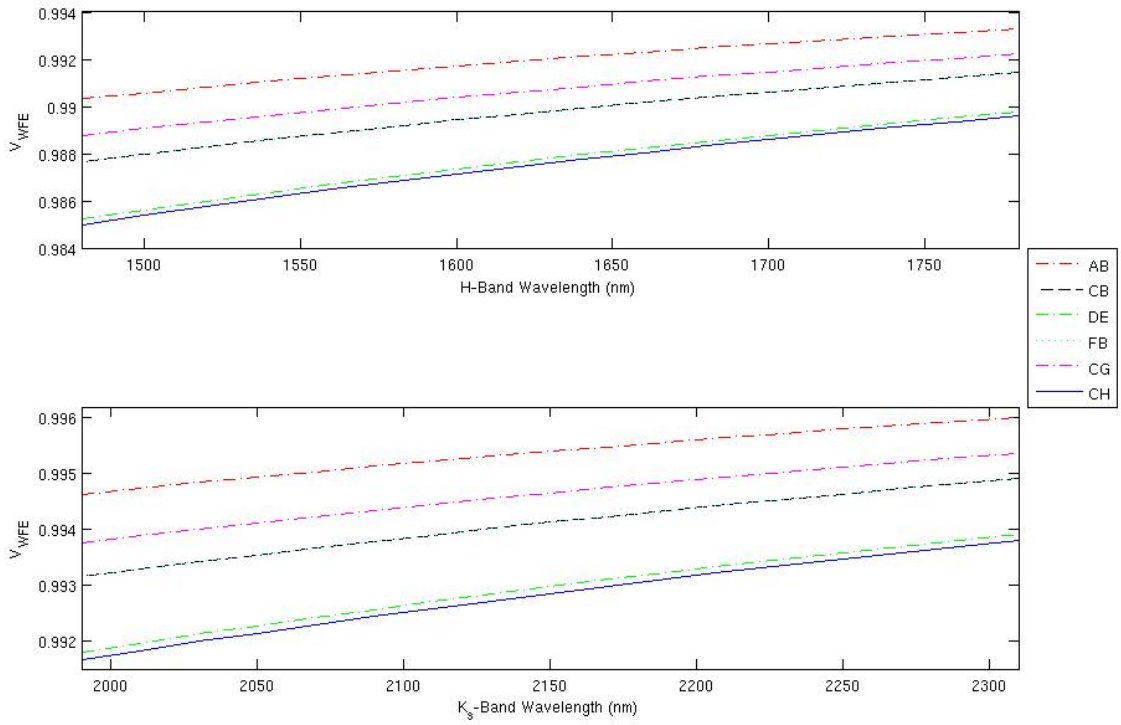

Figure 9. The visibility losses due to wavefront error as a function of wavelength for the H-Band (top) and K_s-Band (bottom).

Table 2. The visibility factors due to group delay effects for all pairs, outputs and polarizations. Group delay visibility losses are very small; the largest reduction in fringe visibility contrast is only 0.8%.

Pair	Band	V_p(RR-LT)	V_s(RR-LT)	V_p(LR-RT)	V_s(LR-RT)
A-B	H	0.996	0.995	1.000	1.000
	K_s	1.000	1.000	0.999	0.999
C-B	H	1.000	1.000	0.998	0.997
	K_s	1.000	1.000	1.000	1.000
D-E	H	1.000	1.000	0.997	0.995
	K_s	1.000	0.999	1.000	1.000
F-B	H	0.998	0.999	0.992	0.993
	K_s	0.996	0.996	0.995	0.995
C-G	H	0.999	0.999	0.994	0.992
	K_s	1.000	1.000	1.000	1.000
C-H	H	1.000	1.000	0.999	0.999
	K_s	0.999	0.999	1.000	1.000

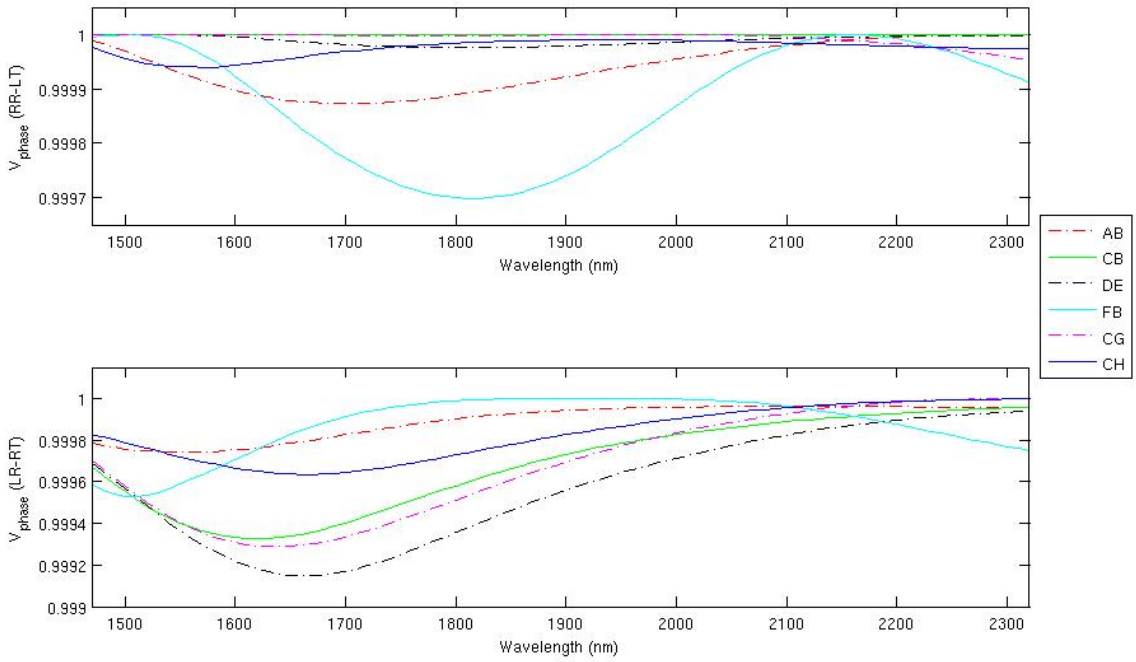

Figure 10. The visibility loss factors due to phase offsets between the interference patterns of the s and p polarization states for combiner outputs (top) RR-LT and (bottom) LR-RT. Note that the vertical scales for the RR-LT and LR-RT outputs graphs are not equal.

of the fringe tracker in practice. In this section we calculate a net visibility factor which takes into account losses as a result of wavefront error, intensity mismatch and polarization effects due to both the combiner architecture and the dielectric coatings. This net visibility factor is denoted as V in Tables 3 and 4 and ranges from about 8% (pair A-B for the LR-RT output in H-Band) to 1% (pair C-B for the RR-LT output in K_s-Band).

In order to determine the visibility loss due to the dielectric coatings alone we have calculated the ratio of the net visibility factor to the ideal visibility that would have been obtained using perfect dielectric coatings. This "ideal" visibility is denoted as V_{ideal} and was determined by calculating the loss in visibility due to intensity mismatches resulting from the combiner architecture alone at the midpoints of the H and K_s bands (1635 nm and 2150 nm, respectively). This ratio of net visibility to ideal visibility is presented in Tables 3 and 4. In the worst case, the reduction of fringe visibilities with respect to the ideal visibility is roughly 3% (pair D-E for the LR-RT output in H-Band). The best case actually represents an increase in fringe visibility contrast over the ideal case of 0.8% (pair C-G for the LR-RT output in H-Band). This slight superiority to the ideal case occurs in four instances in Tables 3 and 4 and is a result of the coating efficiencies counteracting the intensity mismatches arising from the combiner architecture.

Although we have been considering the fringe contrast as a metric for the combiner performance, this does not capture the signal-to-noise losses that any imperfections in the combiner might produce in the measurement of astronomical sources. In this case it is more appropriate to consider the product of the net visibility factor, V, and the detected intensity, I. This quantity is shown in the rightmost column of Tables 2 and 3 and is denoted as VI. These data show that, as expected, VI does not vary significantly between complimentary combiner outputs. Interestingly, the combiner paths with the largest fringe contrast losses correspond to the highest values of VI. This highlights the fact that the largest fringe contrast losses for our combiner always occur when 50% of the light from one of the array telescopes is mixed with 100% of the light from another, the latter not needing to be shared with any other telescope beam. In these cases, although the fringe contrast is reduced, this is more than

Table 3. The net visibility factor (V), ideal visibility (V_{ideal}), net visibility normalized by the ideal case (V/V_{ideal}) and visibility* intensity (VI) for combiner output RR-LT.

Pair (RR-LT)	Band	V	V_{ideal}	V/V_{ideal}	VI
A-B	H	0.944	0.943	1.001	0.708
	K_s	0.943	0.943	1.001	0.708
C-B	H	0.990	1.000	0.990	0.495
	K_s	0.994	1.000	0.994	0.497
D-E	H	0.969	0.980	0.988	0.404
	K_s	0.973	0.980	0.993	0.405
F-B	H	0.966	0.980	0.986	0.403
	K_s	0.973	0.980	0.993	0.406
C-G	H	0.929	0.943	0.985	0.697
	K_s	0.936	0.943	0.993	0.702
C-H	H	0.976	0.980	0.996	0.407
	K_s	0.977	0.980	0.997	0.407

Table 4. The net visibility factor (V), ideal visibility (V_{ideal}), net visibility normalized by the ideal case (V/V_{ideal}) and visibility*intensity (VI) for combiner output LR-RT.

Pair (LR-RT)	Band	V	V_{ideal}	V/V_{ideal}	VI
A-B	H	0.919	0.943	0.975	0.689
	K_s	0.936	0.944	0.993	0.702
C-B	H	0.987	1.000	0.987	0.493
	K_s	0.994	1.000	0.994	0.497
D-E	H	0.951	0.980	0.971	0.396
	K_s	0.968	0.980	0.988	0.403
F-B	H	0.979	0.980	0.999	0.408
	K_s	0.978	0.980	0.998	0.407
C-G	H	0.950	0.943	1.008	0.713
	K_s	0.943	0.943	1.001	0.707
C-H	H	0.962	0.9780	0.982	0.401
	K_s	0.972	0.980	0.992	0.405

compensated for by the higher combined intensity of the interfering light beams. Most importantly, Tables 2 and 3 demonstrate that the effect of coating and substrate imperfections on the combiner performance is very small, accounting to at most a 3.5% loss in the H-Band and a 1% loss in the K_s-Band in fringe contrast as compared to a combiner using perfect optical components.

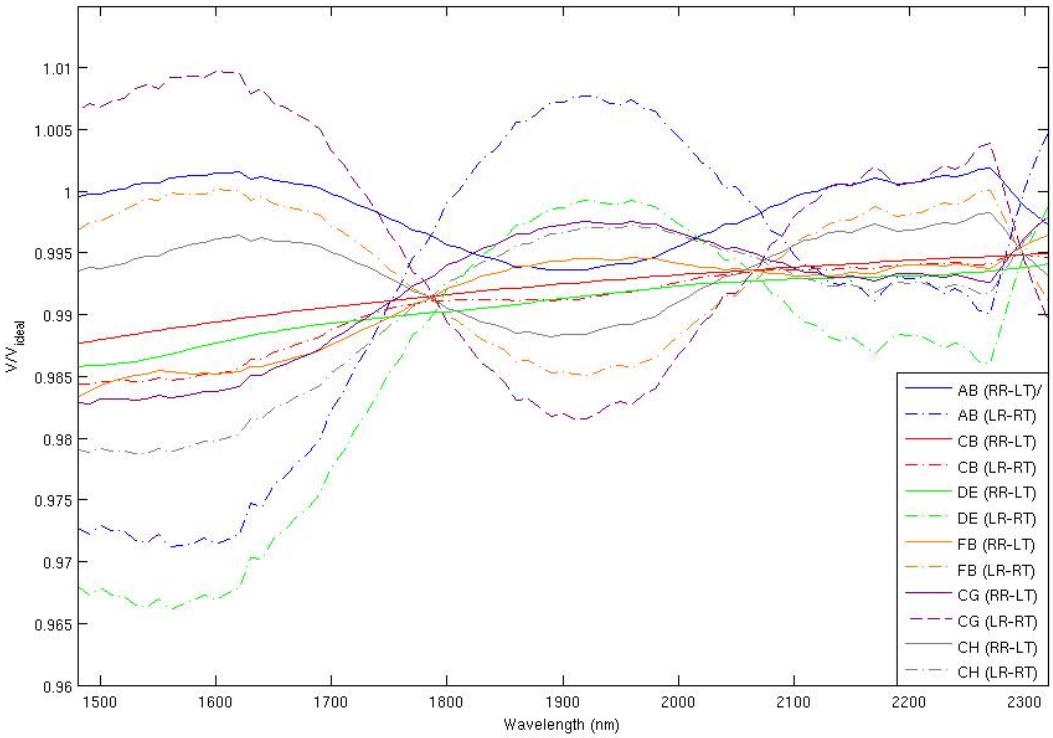

Figure 11. The calculated visibility (V) normalized by the ideal visibility (V_{ideal}). Visibility losses are reduced by at most 3.5% from that of a combiner implementing perfect optics for all wavelengths, pairs and outputs.

6. CONCLUSIONS

We have completed tests on the performance of two out of the three dielectric coatings (the AR and 50% beam-splitter coatings) and calculated the reduction in fringe visibility contrast due to four important factors (intensity mismatch, wavefront error, polarization phase offsets and group delay). The greatest measured visibility losses arise from intensity mismatch (8%) and are mainly due to the beam combiner architecture. Visibility losses due to wavefront error and group delay were both very small with maximum reductions of fringe visibility less than 2% and 0.8%, respectively. Polarization effects had the most insignificant contribution to fringe visibility losses with reductions of 0.10% or less. The net visibility losses due to the combined effects of intensity mismatch, polarization and wavefront error were ∼8% or less for all combination paths due to the coatings and the combiner architecture. We have concluded that the performance of the fringe tracker beam combiner is primarily limited by the system architecture and not the optical coatings or substrates. Overall, the custom coatings for the fringe tracker beam combiner meet the top level science goals for MROI and are well within the error budgets for the overall performance of the array.

ACKNOWLEDGMENTS

The Magdalena Ridge Observatory (MRO) is funded by Agreement No. N00173-01-2-C902 with the Naval Research Laboratory (NRL). MROI is hosted by the New Mexico Institute of Mining and Technology (NMT) at Socorro, NM, USA, in collaboration with the University of Cambridge (UK). Our collaborators at the University of Cambridge wish to also acknowledge their funding via STFC in the UK.

REFERENCES

[1] Creech-Eakman, M.J., Romero, V.D., Cornier, C., Haniff, C.A., Buscher, D.F., and Westpfahl, D.J., "Magdalena Ridge Observatory Interferometer: Advancing to First Light and New Science," *Proc. SPIE* **7734** (2010).

[2] Jurgenson, C.A., Santoro, F.G., McCracken, T., McCord, K., Shtromberg, A., Klinglesmith, D., Olivares, A., Buscher, D.F., Creech-Eakman, M.J., Haniff, C.A., and Young, J.S., "The MROI Fringe Tracker: First Fringe Experiment," *Proc. SPIE* **7734** (2010).

[3] Traub, W.A., "Beam Combination and Fringe Measurement," in [*Principles of Long Baseline Stellar Interferometry*], Lawson, P. R., ed., *Michelson Summer School* (1999).

[4] Armstrong, J., Mozurkewich, D., Pauls, T., and Haiian, A., "Bootstrapping the NPOI: Keeping Long Baselines in Phase by Tracking Fringes on Short Baselines," *Proc. SPIE* **3350** (1998).